

Learning complexity gradually in quantum machine learning models

Erik Recio-Armengol,^{1,2} Franz J. Schreiber,³ Jens Eisert,^{3,4,5} and Carlos Bravo-Prieto³

¹ICFO-Institut de Ciències Fòniques, The Barcelona Institute of Science and Technology, 08860 Castelldefels (Barcelona), Spain

²Eurecat, Centre Tecnològic de Catalunya, Multimedia Technologies, 08005 Barcelona, Spain

³Dahlem Center for Complex Quantum Systems, Freie Universität Berlin, 14195 Berlin, Germany

⁴Fraunhofer Heinrich Hertz Institute, 10587 Berlin, Germany

⁵Helmholtz-Zentrum Berlin für Materialien und Energie, 14109 Berlin, Germany

Quantum machine learning is an emergent field that continues to draw significant interest for its potential to offer improvements over classical algorithms in certain areas. However, training quantum models remains a challenging task, largely because of the difficulty in establishing an effective inductive bias when solving high-dimensional problems. In this work, we propose a training framework that prioritizes informative data points over the entire training set. This approach draws inspiration from classical techniques such as *curriculum learning* and *hard example mining* to introduce an additional inductive bias through the training data itself. By selectively focusing on informative samples, we aim to steer the optimization process toward more favorable regions of the parameter space. This data-centric approach complements existing strategies such as warm-start initialization methods, providing an additional pathway to address performance challenges in quantum machine learning. We provide theoretical insights into the benefits of prioritizing informative data for quantum models, and we validate our methodology with numerical experiments on selected recognition tasks of quantum phases of matter. Our findings indicate that this strategy could be a valuable approach for improving the performance of quantum machine learning models.

In light of the impressive success of classical machine learning and the ever-improving experimental means to perform *quantum computing*, the study of the potential and limitations of *quantum machine learning* (QML) have become a topic of widespread interest. Quantum systems are known to perform learning tasks that are beyond the capabilities of classical computers [1–4]. However, there is growing evidence that the training of quantum learning models is hindered by severe problems not present in classical machine learning. Recent investigations have highlighted that the cost landscape of quantum learning models contains many poor minima and vast regions of vanishing gradients, so-called *barren plateaus*, which preclude trainability [5–11].

To address these training challenges and enhance the performance of quantum learning models, it is crucial to introduce a favorable *inductive bias* [12–14]. Indeed, barren plateaus arise from random initialization in high dimensional problems, where the cost landscape becomes flat, and gradients vanish due to the concentration of measure phenomenon. As such, incorporating a well-advised inductive bias is crucial for achieving reasonable performance. In quantum models, inductive bias has typically been introduced through two main strategies: (1) designing specific quantum circuit architectures that exploit problem symmetries or structures [15–21], and (2) employing smart initialization techniques to set the model parameters near to optimal values, often referred to as *warm-starts* [22–30]. Both approaches aim to facilitate the optimization process toward favorable regions of the parameter space, thereby improving trainability and convergence.

However, these approaches primarily focus on modifying the model architecture or parameter initialization, while the role of training data in introducing inductive bias has been largely overlooked. Traditionally, training examples are presented to the learner in random order, a practice common in both classical and quantum machine learning. Nonetheless, there is an increasing awareness in classical machine learning

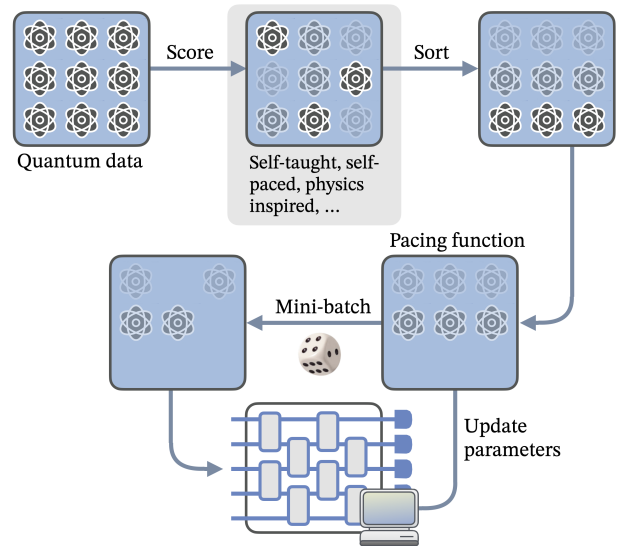


Figure 1. The training framework begins by scoring quantum data points according to a predefined scoring function (e.g., self-taught, self-paced, or physics-inspired). Data points are sorted by score, and the pacing function determines how much of the dataset is accessible at each training epoch. Mini-batches are then sampled from the available subset, and used to update the model parameters iteratively, enabling a gradual change in learning complexity throughout training.

that imposing a specific order on the training data can speed up convergence and lead to better local minima. Typically, this ordering is guided by a *scoring function*, where training starts with examples that have low scores and gradually incorporates data with higher scores as the training progresses. This idea has been explored in different forms, the most prominent examples being *curriculum learning* [31], which was already applied to quantum models [32], and *hard example min-*

ing [33]. These strategies primarily differ in their approach to devising scoring functions. Hard example mining focuses on presenting the learner with difficult examples, while curriculum learning, inspired by human learning processes, starts with easier examples and progressively introduces more challenging ones. Despite their differences, both strategies have demonstrated success across various classical machine learning domains, including *natural language processing*, *computer vision* and others [33–41]. Therefore, adopting an agnostic stance on the design principles is essential, as their quality is ultimately determined by their performance in practice.

Inspired by these powerful classical methods, this work explores an approach to incorporate inductive bias into quantum learning models through the quantum data itself. By carefully selecting, structuring, and presenting the quantum data, we aim to steer the optimization process away from unfavorable regions of the parameter space and guide the model toward better generalization and faster convergence. This data-centric perspective offers a complementary strategy to existing methods focusing on circuit design and parameter initialization. Our contributions include developing a unified and intuitive quantum analog of curriculum learning and hard example mining, tailored to the characteristics of quantum models. Through theoretical analysis and empirical validation, we demonstrate that leveraging the structure and presentation of quantum data can improve the trainability and performance of quantum learning models. This approach not only enhances optimization but also opens new avenues for introducing inductive bias in quantum machine learning. More broadly, our work represents a step toward importing sophisticated methods from classical machine learning into the quantum domain, reflecting the growing maturity of the field.

I. PRELIMINARIES

A. Learning setup and training procedure

We consider a supervised learning scenario involving training data consisting of a collection of quantum state vectors $\{|\psi_i\rangle \in \mathcal{H}\}$ and their respective labels $y_i \in \mathcal{Y} \subseteq \mathbb{R}$. Our quantum learning model, represented as $f_{\vartheta} : \mathcal{H} \rightarrow \mathcal{Y}$, has trainable parameters $\vartheta = (\vartheta_1, \vartheta_2, \dots)$. The training set is denoted by $\mathbb{X} = \{X_i\}_{i=1}^N = \{|\psi_i\rangle, y_i\}_{i=1}^N$. Depending on the specific learning task, the collection of quantum state vectors $\{|\psi_i\rangle\}$ may naturally arise or encode classical training data through a particular embedding process. Our goal is to identify a set of parameters ϑ that minimizes a given loss function $\ell(\vartheta; (|\psi\rangle, y))$.

Traditionally, the entire training dataset \mathbb{X} is accessible from the start of the training. A common approach is to randomize the order of \mathbb{X} , split it into mini-batches, and perform gradient-based optimization. Variations of this setup exist, but typically, the order in which training data is presented to the learner is not prioritized. Here, we deviate from this conventional setup by initially limiting the learner to a subset of the training data, gradually increasing access to the full dataset.

This framework can be visualized in Fig. 1.

Practically, this is done by introducing a scoring and pacing function. The scoring function determines the order in which data points are added to the subset accessible to the learner by assigning a score $s(|\psi\rangle)$ between 0 and 1 to each data point $|\psi\rangle$.

Definition 1 (Scoring function). *Given a dataset $\{x_i, y_i\}_{i=1}^N$ with $x_i \in \mathcal{X}$, a scoring function is defined as $s : \mathcal{X} \rightarrow [0, 1]$.*

For two data points x_i and x_j , if $s(x_i) \leq s(x_j)$, then x_j should not be available to the learner before x_i . The pacing function essentially dictates the rate at which new data becomes available to the learner by assigning to each epoch a fraction of the training data. Importantly, our framework is also immediately compatible with training on classical data. For example, some methods embed classical data into quantum states, while others, such as data re-uploading [42, 43], encode it directly into quantum circuits. Our framework accommodates such approaches, as the scoring function can operate on either the classical data or their corresponding embedding quantum states without conceptual inconsistency.

Definition 2 (Pacing function). *Let $\mathbb{T} := \{1, 2, \dots, T\}$ enumerate the T training epochs. A pacing function is defined as a function $p : \mathbb{T} \rightarrow [0, 1]$.*

Therefore, in epoch t , the learner has access to the fraction $p(t)$ of the entire dataset based on the scores of $s(|\psi\rangle)$.

B. Scoring and pacing functions

Scoring functions evaluate the training data, often guided according to notions of difficulty or complexity. While we take an agnostic stance on the idea of scoring functions as difficulty measures, it is noteworthy that those inspired by complexity or difficulty, as previously mentioned, have a successful track record in classical machine learning, often capturing data structures that enable better learning.

We briefly review scoring functions used in practice, distinguishing between *domain-agnostic* and *domain-specific* methods. Domain-agnostic scoring functions, despite their name, are typically tied to the training set and are often learned. This involves initially training a secondary learner on the data and using the resulting loss values as a scoring metric. For example, a learner f_{ϑ} may first undergo conventional training, and its hypothesis is subsequently used as a scoring function. Alternative architectures, such as *support vector machines*, can also be adapted in this way. However, this approach can be computationally intensive due to the additional learner.

To mitigate such costs, *self-paced learning* offers a simpler alternative. Here, the loss ℓ_{ϑ} of the current hypothesis f_{ϑ} acts as the scoring function ordering the training data of the subsequent epoch. This method preserves the domain-agnostic nature of scoring while avoiding the overhead of training an auxiliary learner. In contrast, domain-specific scoring functions leverage domain expertise to define metrics, often inspired, as mentioned previously, by complexity measures such

as input length in text-based tasks or the number of objects in an image.

Unlike scoring functions, pacing functions dictate the rate at which training examples are introduced. They are generally domain-agnostic and are chosen to be monotonically increasing. Linear pacing functions are the most common baseline, but non-linear alternatives, such as the *root-p* and *geometric progression* functions [34, 39, 44], are also employed. These can be categorized by their growth relative to linear functions: slower-growing functions textured training on high-scoring examples while faster-growing ones prioritize low-scoring data.

II. RESULTS

A. Analytical insights

In this section, we aim to provide theoretical justification for the use of this learning setup. Specifically, we demonstrate how a learning setup defined by a scoring function s and a pacing function p can address challenges during early training epochs and improve convergence rates. We show that carefully selecting and ordering training data can enhance the training dynamics of parameterized quantum models.

Proposition 1 (Mitigation of barren plateaus). *Let $\{|\psi_i\rangle \in \mathcal{H}\}$ be a collection of quantum state vectors. Let $f_{\vartheta} : \mathcal{H} \rightarrow \mathcal{Y}$ be a parameterized quantum model with parameters $\vartheta \in \Theta$ and $\mathcal{Y} \subseteq \mathbb{R}$ the label space. Consider a loss function $\ell(\vartheta; (|\psi\rangle, y))$ associated with data points $\{(|\psi_i\rangle, y_i) \in \mathcal{H} \times \mathcal{Y}\}$. Suppose there exists a scoring function $s : \mathcal{H} \rightarrow [0, 1]$ such that the expected squared norm of the gradient*

$$G(z) = \mathbb{E} \left[\|\nabla_{\vartheta} \ell(\vartheta; (|\psi\rangle, y))\|^2 \mid s(\psi) = z \right] \quad (1)$$

is a non-increasing function of s . Then, this learning setup defined by s increases the expected squared gradient magnitude during early training epochs compared to standard training (random data order).

The proof is given in Appendix A. By prioritizing data points with lower scores—corresponding to higher expected squared gradient norms—we mitigate the effects of barren plateaus during the initial stages of training. We later give an explicit example of a physically-inspired scoring function s such that Proposition 1 holds. Next, we show that this learning setup could also improve the convergence of the model.

Proposition 2 (Faster convergence). *Let $\{|\psi_i\rangle\} \in \mathcal{H}$ be a collection of quantum state vectors. Let $f_{\vartheta} : \mathcal{H} \rightarrow \mathcal{Y}$ be a parameterized quantum model with parameters $\vartheta \in \Theta$ and $\mathcal{Y} \subseteq \mathbb{R}$ the label space. Consider a convex loss function with Lipschitz continuous gradients $\ell(\vartheta; (|\psi\rangle, y))$ associated with data points $\{(|\psi_i\rangle, y_i) \in \mathcal{H} \times \mathcal{Y}\}$. Suppose there exists a scoring function $s : \mathcal{H} \rightarrow [0, 1]$ such that the scoring function $s(|\psi\rangle)$ prioritizes data points with lower gradient variance at each epoch, and the pacing function p increases monotonically over epochs $t = 1$ to T . Then, this learning setup defined by s and p results in a lower expected empirical risk after T*

epochs compared to standard training (random data order), i.e.,

$$\mathbb{E}[R(\vartheta_T^{s,p})] \leq \mathbb{E}[R(\vartheta_T^{rand})] \quad (2)$$

where $R(\vartheta) := \frac{1}{N} \sum_{i=1}^N \ell(f_{\vartheta}; (|\psi_i\rangle, y_i))$ is the empirical risk, and N the batch size.

The proof is given in Appendix B. By selecting data points with lower gradient variance, more stable and efficient updates are achieved during training. The assumption of Lipschitz continuity for the gradients assumption is reasonable, given that the empirical risk $R(\vartheta)$ is generally bounded. The convexity assumption ensures a well-behaved loss landscape, which, while not always realistic, makes the analysis tractable. However, this assumption might be particularly reasonable in scenarios where this learning setup is combined with other warm-start techniques that initialize the parameters near to optimal values. By employing a scoring function that prioritizes such data points and a pacing function that gradually increases the complexity of the training set, the learning process can benefit from reduced variance in gradient estimates, resulting in faster convergence and lower expected risk after a fixed number of epochs.

While these propositions provide a theoretical intuition for the use of hard example mining and curriculum learning in quantum machine learning, empirical validation remains crucial. The theoretical benefits outlined may vary in practice due to factors such as the specific architecture of the quantum model, the characteristics of the data distribution, and the optimization algorithm used. Constructing meaningful scoring and pacing functions remains challenging, and empirical experiments are essential for assessing the practical effectiveness of this learning setup. Such validation can help identify discrepancies between expected and observed performance, allowing adjustments to optimize the approach for specific applications. Interestingly, although Propositions 1 and 2 lay the theoretical ground for what to expect, the numerical performance in certain cases significantly exceeds these initial insights.

B. Numerical results

The methodology and underlying principles presented here are generally applicable to quantum machine learning tasks. For specificity, however, we focus on phase recognition. This section presents numerical results demonstrating the application of the presented framework to quantum phase recognition, a popular benchmark task in QML [45–50] due to its importance in the study of condensed matter physics [51, 52]. We explore its effectiveness on two paradigmatic quantum spin chains: the *generalized cluster model* and the *bond-alternating XXZ model*, both well-studied quantum many-body Hamiltonians.

The *generalized cluster model* is described by the following

local Hamiltonian

$$H_{\text{cluster}} = \sum_{j=1}^n (Z_j - j_1 X_j X_{j+1} - j_2 X_{j-1} Z_j X_{j+1}), \quad (3)$$

where n is the number of qubits, j_1 and j_2 are coupling strengths, and X_i and Z_i are Pauli operators acting on the i^{th} qubit. As shown in Refs. [53, 54], and illustrated in Fig. 2(a), the ground-state phase diagram exhibits four distinct regimes: (I) a symmetry-protected topological phase, (II) a ferromagnetic phase, (III) an anti-ferromagnetic phase, and (IV) a trivial phase. For specific choices of parameters, this Hamiltonian is the standard cluster model, the conventional cluster state being the ground state.

The *bond-alternating XXZ Hamiltonian* is slightly more complicated, although it remains geometrically local, and reads

$$H_{\text{XXZ}} = j_1 \sum_{j=1}^{n/2} (X_{2j-1} X_{2j} + Y_{2j-1} Y_{2j} + \delta Z_{2j-1} Z_{2j}) + j_2 \sum_{j=1}^{n/2-1} (X_{2j} X_{2j+1} + Y_{2j} Y_{2j+1} + \delta Z_{2j} Z_{2j+1}), \quad (4)$$

where j_1 and j_2 are coupling strengths, X_i , Y_i and Z_i are Pauli operators acting on the i^{th} qubit, and δ is the spin anisotropy. As depicted in Fig. 2(b), this model Hamiltonian hosts three distinct phases that can be detected by the many-body topological invariant $\mathcal{Z}_{\mathcal{R}}$ [55]: (I) a trivial phase, (II) a symmetry-broken antiferromagnetic phase, and (III) a topological phase.

Our learning tasks involve developing a classification model that can identify the quantum phase given the ground state of a system described by either the *generalized cluster Hamiltonian* or the *bond-alternating XXZ Hamiltonian*. We achieve this by generating a training set, denoted by $S = \{(|\psi_i\rangle, \mathbf{y}_i)\}_{i=1}^N$, where N represents the number of training data points. Each element in S is a pair: $|\psi_i\rangle$ corresponds to the ground state vector of the Hamiltonian (H_{cluster} or H_{XXZ}) for a specific choice of coupling constants (j_1 and j_2 or j_1/j_2 and δ). The ground states are drawn from a distribution \mathcal{D} which corresponds to sampling these coupling constants uniformly at random, ensuring a balanced representation of all classes. The second element, \mathbf{y}_i , represents the corresponding one-hot encoded phase label. In this scheme, each label is a vector with a length equal to the number of classes, with only one element set to 1, indicating the corresponding phase.

We leverage the *quantum convolutional neural network* (QCNN) architecture introduced in Ref. [56] for the phase classification tasks. Inspired by classical convolutional neural networks, QCNNs are expected to excel at identifying spatial or temporal patterns, making them well-suited for this purpose. A key feature of QCNNs is their alternating structure of convolutional and pooling layers. Convolutional layers apply parameterized, translation-invariant unitary operations to neighboring qubits, acting like filters between feature maps across layers. Pooling layers then reduce the dimensionality of the quantum state while preserving the relevant information. This is achieved by measuring a subset of qubits and

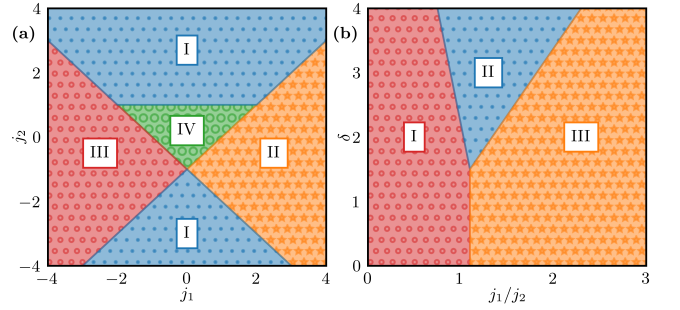


Figure 2. Ground-state phase diagrams of (a) the *generalized cluster Hamiltonian* in Eq. (3), exhibiting (I) symmetry-protected topological, (II) ferromagnetic, (III) anti-ferromagnetic, and (IV) trivial phases; and (b) the *bond-alternating XXZ Hamiltonian* in Eq. (4), displaying (I) trivial, (II) symmetry-broken antiferromagnetic, and (III) topological phases.

applying single-qubit unitaries based on the measurement outcomes. Each pooling layer consistently reduces the number of qubits by a constant factor, leading to quantum circuits with logarithmic depth compared to the initial system size.

We can describe the action of the QCNN as a quantum channel \mathcal{C}_{ϑ} parameterized by ϑ . This channel transforms an input state ρ_{in} into an output state ρ_{out} via the mapping $\rho_{\text{out}} = \mathcal{C}_{\vartheta}[\rho_{\text{in}}]$. Following this, a task-specific Hermitian operator is measured on the output state ρ_{out} to obtain an expectation value. In our numerical implementations, the QCNN maps an 8-qubit input state vector $|\psi\rangle$ into a 2-qubit output state. The labeling function for the output state utilizes the probabilities obtained by measuring the state in the computational basis, giving rise to outcomes (0, 0), (0, 1), (1, 0), (1, 1). Specifically, the predicted label $\hat{\mathbf{y}}$ corresponds to the vector of the probabilities as defined by

$$|\psi\rangle \mapsto (p_j)_{j \in \{0,1\}^2} \mapsto \hat{\mathbf{y}} := (p_{0,0}, p_{0,1}, p_{1,0}, p_{1,1}). \quad (5)$$

For each experimental run, data is generated from the corresponding distribution \mathcal{D} . During training, we employ the mean squared error as loss function

$$\ell(\vartheta; (|\psi\rangle, \mathbf{y})) := \sum_{j=1}^M (\langle j | \mathcal{C}_{\vartheta} [|\psi\rangle\langle\psi|] |j\rangle - y_j)^2, \quad (6)$$

where M is the number of classes. Then, given a training set of size N drawn from the distribution \mathcal{D} , we sample a mini-batch of size L , and we minimize the empirical risk

$$\hat{R}_S(\vartheta) = \frac{1}{L} \sum_{i=1}^L \ell(\vartheta; (|\psi_i\rangle, \mathbf{y}_i)). \quad (7)$$

Let us detail here the experimental setup used throughout the following sections. We generate a training set S containing 50 ground states drawn from the distribution \mathcal{D} , and a test set T containing 1000 samples from the same distribution. We refer to the standard approach of uniformly sampling mini-batches of size L from the training set S as the

standard method. In this work, we use a fixed mini-batch size of $L = 10$. Next, we define a scoring function $s : S \rightarrow \mathbb{R}$ to measure the difficulty of each training example $(|\psi_i\rangle, \mathbf{y}_i)$. This function assigns a higher score to harder examples, e.g., $s(|\psi_i\rangle, \mathbf{y}_i) > s(|\psi_j\rangle, \mathbf{y}_i)$. The scoring function s incorporates prior knowledge and thus embodies some of the inductive bias of the model. We additionally define a pacing function to determine how the size of the subsets from which mini-batches are uniformly sampled is adjusted throughout training. Details regarding the specific pacing functions employed are provided in Ref. [57].

For the quantum circuit simulations, we leverage the PennyLane [58] software library running on classical hardware. We utilize the ADAM optimizer [59] for parameter updates during training, which is a stochastic gradient descent method that dynamically adjusts learning rates.

1. Self-taught learning

In this first experiment, we order the quantum data based on the loss of a pre-trained QCNN model with identical architecture and trained without ordering. This is usually referred to as *self-taught* learning. At the beginning of the training, we order the training set according to the loss of each data point. We then gradually increase the number of data points used for training throughout the epochs, following a monotonically increasing pacing function. We consider four orderings: (1) *Standard*, which is used as a baseline and corresponds to the standard approach with no specific ordering nor pacing function, all data points are treated equally from the start; (2) *Random*, where data points are randomly ordered, and serves as a control that should behave similar to the Standard approach; (3) *Easy*, which prioritizes data points with lower loss values (easier examples); and (4) *Hard*, which prioritizes data points with higher loss values (harder examples).

Figure 3 shows the average performance over ten runs of these strategies on the *generalized cluster* and the *bond-alternating XXZ models*. For both spin models, the Standard and Random strategies exhibit comparable performance, achieving the best accuracy nearing 80%. This similarity arises because Random introduces random ordering, mirroring the uniform treatment of data in the Standard approach. Interestingly, the Easy strategy, which prioritizes easier examples, performs worse than both Standard and Random, converging to a lower accuracy and suggesting that early exposure to easier examples might not be optimal. Conversely, the Hard strategy, which focuses on harder examples, despite initially slower convergence, ultimately yields the best performance, approaching 90% accuracy (see Table I). Notably, for the *bond-alternating XXZ model* shown in Fig. 3(b), the highest accuracy is reached before the end of the training and then it decreases in the final optimization steps due to the incorporation of the easiest examples in the training batch. This suggests that exposure to non-informative data points might even be detrimental for the performance of the quantum model, and highlights the potential benefit of focusing on complex examples early in the training.

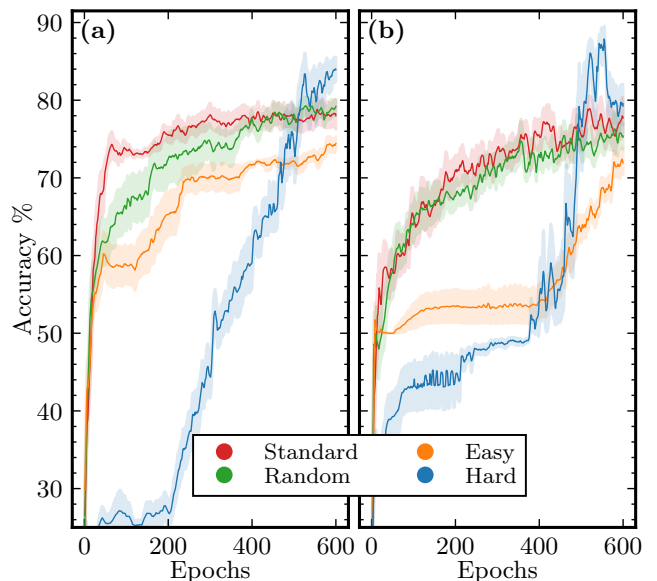


Figure 3. Average accuracy on the test set as a function of the training epochs for the quantum phase recognition task for the (a) *generalized cluster model* and (b) the *bond-alternating XXZ model*, using a self-taught strategy. The shaded areas represent the standard error of the mean over ten runs with different random initialization and training data.

	Generalized cluster		Bond-alternating XXZ	
	Training (%)	Test (%)	Training (%)	Test (%)
<i>Standard</i>	79.4	78.2	81.2	78.6
<i>Random</i>	80.6	79.2	78.8	75.8
<i>Easy</i>	75.6	74.4	73.4	72.4
<i>Hard</i>	86.6	83.6	88.0	86.5

Table I. Average best accuracy over ten runs for the quantum phase recognition task on the *generalized cluster model* and the *bond-alternating XXZ model*, using a self-taught strategy. The best-performing method prioritizes hard examples early in the training.

2. Self-paced learning

Self-paced learning dynamically prioritizes training data based on the performance of the current model, unlike the self-taught strategy which scores each point based on the loss with respect to the target hypothesis. In this approach, we rank the training set by the current loss of each data point at each epoch. We explore four strategies within this framework, using a monotonically increasing pacing function to gradually expose more data points as training progresses: (1) *Standard*, (2) *Easy*, and (3) *Hard*, which we discussed previously, and (4) *Hardest*, which employs a constant pacing function, consistently training on the ten most difficult examples at each epoch. This means that, although the pacing function is constant, the most difficult examples can vary at each epoch depending on the performance of the model.

The performance of these strategies is illustrated in Fig. 4,

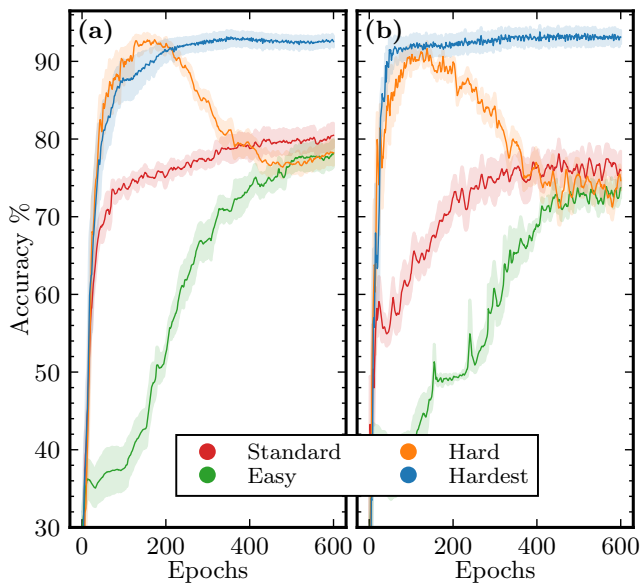


Figure 4. Average accuracy on the test set as a function of the training epochs for the quantum phase recognition task for the (a) *generalized cluster model* and (b) the *bond-alternating XXZ model*, using a self-paced strategy. The shaded areas represent the standard error of the mean over ten runs with different random initialization and training data.

showing the average accuracy on the training and test sets for the quantum phase recognition task across the two spin models. Standard and Easy strategies achieve similar performance, with a final accuracy nearing 80%. This indicates that a straightforward or Easy approach does not significantly boost the model’s learning capability. The Hard strategy initially shows promising performance but regresses as more data points are introduced due to the increasing pacing function. Despite this regression, it demonstrates the potential benefit of focusing on complex examples early in the training. In striking contrast, the Hardest strategy quickly converges to near-perfect accuracy on the training set and achieves over 90% accuracy on the test set (see Table II). By consistently training on the hardest examples, the model develops a robust understanding of the most challenging aspects of the training data, such as the boundaries of the different quantum phases—as we further explore in Sec II B 4—hence significantly enhancing its performance.

3. Physics-inspired learning

A key difference between classical and quantum machine learning is, once again, the presence of barren plateaus, where the variation of the loss function over the parameter landscape is exponentially suppressed with the system size [6]. At its core, this is a concentration of measure effect in high dimensions and can be captured in several different ways. One effective approach is through the *dynamical Lie algebra* (DLA) of the circuit ansatz [5, 60]. The DLA \mathfrak{g} is defined as the Lie

	Generalized cluster		Bond-alternating XXZ	
	Training (%)	Test (%)	Training (%)	Test (%)
<i>Standard</i>	83.2	77.4	82.2	77.4
<i>Easy</i>	80.8	78.1	76.4	73.5
<i>Hard</i>	98.6	92.6	95.0	91.6
<i>Hardest</i>	99.8	92.6	97.2	93.5

Table II. Average best accuracy over ten runs for the quantum phase recognition task on the *generalized cluster model* and the *bond-alternating XXZ model*, using a self-paced strategy. The best-performing method prioritizes the hardest examples in each training epoch.

closure over its set of generators,

$$\mathfrak{g} := \langle i\mathcal{G} \rangle_{\text{Lie}}, \quad (8)$$

where the generators are the generators of the parametrized gates of the circuit, $\mathcal{G} := \{H_1, H_2, \dots, H_K\}$. The DLA \mathfrak{g} is the vector space (over \mathbb{R}) that is obtained by taking the span over all the nested commutators that can be formed from the elements of $i\mathcal{G}$. Assuming that the quantum neural network approximates a unitary 2-design [61] over the unitary group generated by the DLA \mathfrak{g} , for the training state ρ , the variation of the loss is then given by

$$\text{Var}(\ell(\boldsymbol{\theta}; \rho, O)) = \frac{\mathcal{P}_{\mathfrak{g}}(\rho)\mathcal{P}_{\mathfrak{g}}(O)}{\dim(\mathfrak{g})}, \quad (9)$$

where $\mathcal{P}_{\mathfrak{g}}$ denotes the \mathfrak{g} -purity, defined for Hermitian operators as

$$\mathcal{P}_{\mathfrak{g}}(H) := \sum_{l=1}^{\dim(\mathfrak{g})} \left| \text{Tr}(B_l^\dagger H) \right|^2. \quad (10)$$

Here, $\{B_j\}_{j=1}^{\dim(\mathfrak{g})}$ is a Hilbert-Schmidt orthonormal basis of the vector space $\mathfrak{g}_{\mathbb{C}} := \text{span}(\mathfrak{g})$. From Eq. (9) we observe that barren plateaus occur if either $1/\dim(\mathfrak{g}) = \mathcal{O}(b^{-n})$, $\mathcal{P}_{\mathfrak{g}}(O) = \mathcal{O}(b^{-n})$ or $\mathcal{P}_{\mathfrak{g}}(\rho) = \mathcal{O}(b^{-n})$ with $b > 1$.

The only term in Eq. (9) that depends on the training data is the \mathfrak{g} -purity given in Eq. (10). Favorable scaling of this quantity is a necessary condition to avoid an exponentially vanishing variance in Eq. (9) and, consequently, the onset of barren plateaus. Since one of the key statistical assumptions of barren plateaus is a random initialization of the trainable parameters, their appearance is most accurate at the beginning of training. Particularly during this initial training phase, one can expect that training data with higher \mathfrak{g} -purity enhances the trainability of the model, as these points are associated, on average, with larger gradients in the asymptotic regime. This, however, does not necessarily hold for finite system sizes, as barren plateaus are an intrinsically asymptotic concept. Building on this intuition, we propose the following domain-specific scoring function

$$s(\rho) = 1 - \mathcal{P}_{\mathfrak{g}}(\rho) \quad (11)$$

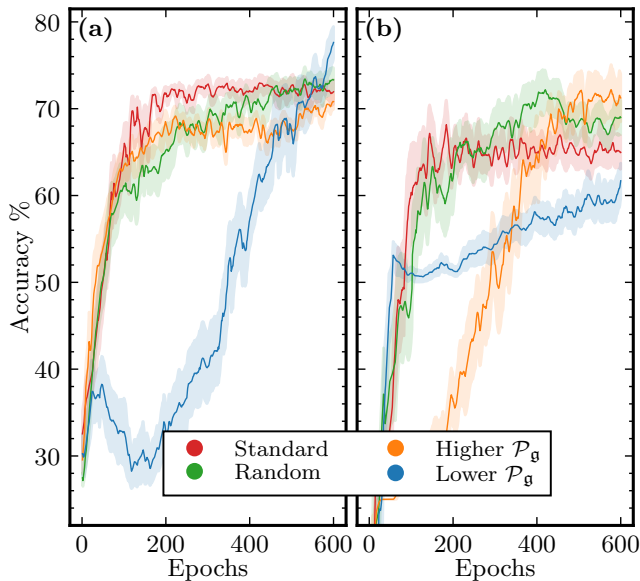


Figure 5. Average accuracy on the test set as a function of the training epochs for the quantum phase recognition task for the (a) *generalized cluster model* and (b) the *bond-alternating XXZ model*, using a physics-inspired strategy (\mathcal{P}_g of the training quantum states). The shaded areas represent the standard error of the mean over ten runs with different random initialization and training data.

	Generalized cluster		Bond-alternating XXZ	
	Training (%)	Test (%)	Training (%)	Test (%)
<i>Standard</i>	71.6	72.5	70.0	67.9
<i>Random</i>	72.8	72.9	73.8	71.9
<i>Higher \mathcal{P}_g</i>	68.6	70.9	73.4	71.6
<i>Lower \mathcal{P}_g</i>	78.6	77.2	62.4	60.8

Table III. Average best accuracy over ten runs for the quantum phase recognition task on the *generalized cluster model* and the *bond-alternating XXZ model*, using a physics-inspired strategy.

where lower scores correspond to training examples with high g -purity, which are prioritized at the beginning of training. Notice that choosing s this way ensures that Proposition 1 holds. Accordingly, as training progresses and the model converges to more favorable regions of the cost landscape, the statistical assumptions underpinning barren plateaus become less relevant. As this occurs, we gradually incorporate more training data with higher scores, which correspond to lower g -purity. Ideally, this way, the model can still learn from the complete training set without low gradient data points impeding the training progress.

A potential limitation of using g -purity as a score function for larger system sizes is the computational difficulty associated with calculating \mathcal{P}_g , which generally scales exponentially with the number of qubits. To address this challenge, it is worthwhile to explore approximation schemes for computing \mathcal{P}_g , which could have broader implications beyond our specific context, particularly for understanding when quantum

systems can be efficiently simulated using Lie-algebraic techniques [62]. To this end, we note that there are two sources of computational hardness. First, the Lie algebra itself might be exponentially large, requiring an exponentially sized basis of \mathfrak{g}_C . In such cases, training would likely be infeasible anyway, as then $1/\dim(\mathfrak{g}) = \mathcal{O}(b^{-n})$. Second, even if the dimension of the Lie algebra grows only polynomially in the system size, that does not guarantee an efficient method for finding a basis for the space \mathfrak{g}_C . Computing the basis elements $\{B_j\}_{j=1}^{\dim(\mathfrak{g})}$ requires computing nested commutators of the generators in $i\mathcal{G}$ and verifying the linear independence the resulting operators (c.f. Algorithm 1 in Ref. [63]). While we have an efficient classical description of the generating set, this does not ensure that the required operations (nested commutators and linear independence checks) can be performed efficiently. Instead, we may need to represent the generators as elements of \mathbb{C}^{2^n} to carry out these computations, making the determination of even a single basis element B_j quickly infeasible. There are, however, special cases in which efficient procedures for computing $\{B_j\}_{j=1}^{\dim(\mathfrak{g})}$ are known [5, 62].

To avoid computational bottlenecks in this section, we simplified the QCNN while preserving its structure to a parameterized matchgate circuit composed of fermionic Gaussian unitaries. Specifically, the circuit generators are $\mathcal{G} = \{Z_i\}_{i=1}^8 \cup \{X_i X_{i+1}\}_{i=1}^7$, producing a DLA \mathfrak{g} that remains computationally feasible. This simplification results in a QCNN with fewer variational parameters, leading to reduced performance across all strategies. Nonetheless, this trade-off is acceptable because our goal is not to optimize performance but rather to compare differences between frameworks (e.g., Standard versus alternative methods). We consider four strategies: (1) *Standard* and (2) *Random*, previously discussed, and (3) *Higher \mathcal{P}_g* and (4) *Lower \mathcal{P}_g* , which prioritize higher and lower \mathcal{P}_g states early in the training, respectively.

Figure 5 shows the accuracy performance of these strategies on the training and test sets for our quantum phase recognition tasks. We observe different behaviors for each spin model under study. For the *generalized cluster model*, the Standard and Random strategies perform similar, as expected. Interestingly, the Higher \mathcal{P}_g also performs similarly, though with slightly worse results. Conversely, the Lower \mathcal{P}_g strategy shows a gradual improvement initially, eventually achieving the highest performance on both test and training sets (see also Table III).

In contrast, for the *bond-alternating XXZ model*, while the Standard and Random strategies exhibit similar performance to those observed in the *generalized cluster model*, the \mathcal{P}_g -based strategies behave differently. In this case, the final accuracy of the Higher \mathcal{P}_g strategy surpasses that of the Lower \mathcal{P}_g strategy, which significantly underperforms compared to the other strategies. Notably, despite the Higher \mathcal{P}_g strategy achieving the best final accuracy, the highest accuracy during the training is attained by the Random strategy, indicating that this specific implementation does not benefit from \mathcal{P}_g ordering for this particular task.

These results suggest that ordering the quantum data according to \mathcal{P}_g does not consistently yield major improvements in learning performance in this particular setup. While order-

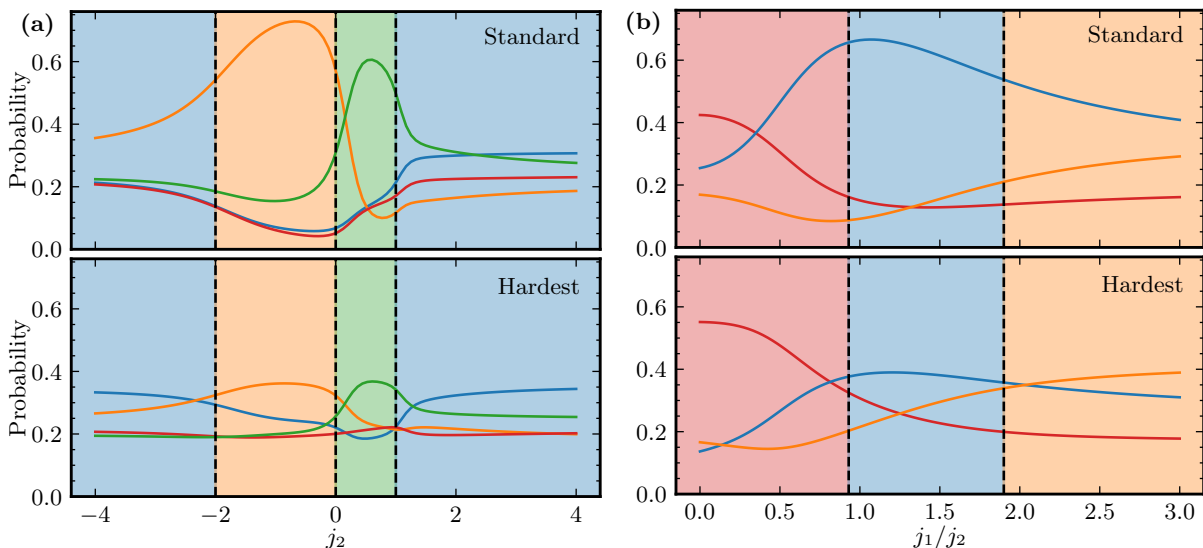


Figure 6. (a) The *generalized cluster Hamiltonian* and (b) *bond-alternating XXZ Hamiltonian* for Standard (top) and Hardest (bottom) strategies. The background color of each panel indicates the true quantum phase of the system. A correct classification occurs when the highest probability color matches the background color of the panel. The self-paced Hardest strategy demonstrates superior accuracy both within each phase region and at the phase boundaries.

ing based on \mathcal{P}_g guarantees larger gradients on average at the early stages of the training, it does not necessarily lead to better learning outcomes. However, it is evident that \mathcal{P}_g captures meaningful properties of the problem, as the performance of the model varies significantly with different orderings. Further research could be beneficial to understand the impact of \mathcal{P}_g on training and to develop a scoring function that may leverage its properties in a non-trivial manner.

4. Accuracy at the cost of confidence

In this section, we try to understand further the differences between the Standard approach and the best-performing method within the proposed framework: the self-paced Hardest learning strategy. We analyze the probabilities for the different phases as determined by the QCNN along a specific cut in the phase diagram in Fig. 2.

We begin by considering the *generalized cluster Hamiltonian*. We focus on a cut along the j_2 coupling constant, fixing $j_1 = 1$. The model undergoes three phase transitions: (1) from symmetry-protected topological to ferromagnetic at $j_2 = 2$, (2) from ferromagnetic to trivial at $j_2 = 0$, and (3) from trivial to symmetry-protected topological at $j_2 = 1$. Figure 6(a) illustrates the probabilities for the different phases under both the Standard (top) and self-paced Hardest (bottom) strategies. The phase diagram is accurately captured by the QCNN trained with the self-paced strategy, whereas the Standard approach fails to precisely detect the phase boundaries.

Next, we examine the *bond-alternating XXZ Hamiltonian*. Here, we zoom-in cut along the j_1/j_2 coupling constants, fixing $\delta = 3$. The model features two phase transitions: (1) from trivial to symmetry-broken antiferromagnetic at $j_1/j_2 \approx 1$,

and (2) from symmetry-broken antiferromagnetic to topological at $j_1/j_2 \approx 2$. Figure 6(b) shows the probabilities for the different phases under both the Standard (top) and self-paced Hardest (bottom) strategies. Once again, the QCNN trained with the self-paced strategy accurately captures the phase diagram, while the Standard approach misclassifies a large fraction of the ground states.

Overall, the Hardest approach outperforms the Standard strategy in terms of accuracy, both within individual phases and the phase boundaries. However, it is worth noting that the Hardest approach exhibits less confidence in its predictions, as indicated by the smaller differences between the probabilities of different classes. This suggests a potential trade-off between accuracy and prediction confidence. Despite its superior performance, we still observe slight deviations in the predicted transition points from the actual phase boundary. This discrepancy is expected due to the relatively large correlation length near the phase boundary, which exceeds what the capacity of the 8-qubit QCNN can capture accurately.

III. DISCUSSION

In this work, we have introduced a training approach for quantum machine learning models that leverages the structure of the training data itself to introduce additional inductive bias, thereby improving learning capabilities. Drawing inspiration from classical methods like curriculum learning and hard example mining, we developed a framework tailored to quantum models. We provided some analytical insights and extensive numerical evidence that demonstrates how strategically ordering the quantum data can significantly improve the performance of quantum models.

Analytically, we show the potential of data ordering to ease barren plateaus and enhance convergence. Our numerical experiments, focused on the task of quantum phase recognition in quantum spin chains, further validated the approach. In particular, we observed that prioritizing harder data points early in the training process leads to superior performance compared to traditional training methods. The self-paced learning strategy, which dynamically adjusts data presentation based on current performance, proved to be particularly effective, consistently achieving higher accuracy than other strategies. This emphasizes the potential of data ordering in quantum models, not just as a theoretical concept but as a relevant factor in practical applications.

While the framework presented here showcases interesting results, it also opens up several avenues for future research. One possible direction is to extend these methods to tasks beyond quantum phase recognition, such as unitary learning [45, 64–67] or quantum error correction [56, 68]. Furthermore, exploring different complexity measures—such as those based on notions of entanglement—or combining multiple complexity metrics, including those used in this work, could help refine the scoring and pacing functions. Integrating this data-centric approach with other warm-start techniques, such as those focused on parameter initialization, could further enhance model performance. On a higher level, this work further reinforces the importance of data-centric inductive biases in quantum machine learning models, suggesting that advancing this concept could lead to more sophisticated quantum circuit design strategies that can optimize performance

from the outset, while also underscoring the value of leveraging established classical machine learning methods to foster meaningful progress in quantum machine learning.

CODE AND DATA AVAILABILITY

The code and data generated during the current study are available in Ref. [57].

ACKNOWLEDGMENTS

The authors would like to thank Elies Gil-Fuster and Adrián Pérez-Salinas for useful feedback on a previous version of this manuscript. E. R.-A. acknowledges funding from the Government of Spain (Severo Ochoa CEX2019-000910-S, FUNQIP, and European Union NextGenerationEU PRTR-C17.I1), Fundació Cellex, Fundació Mir-Puig, Generalitat de Catalunya (CERCA program) and European Union (PASQuanS2.1, 101113690). E. R.-A. is a fellow of Eurecat’s “Vicente López” PhD grant program. F. J. S., J. E., and C. B.-P. are supported by the BMBF (MUNIQC-Atoms, Hybrid), the BMWK (EniQma), the Munich Quantum Valley (K-8), the Quantum Flagship (PasQuans2, Millenion), the Einstein Foundation (Einstein Research Unit on Quantum Devices), Berlin Quantum, and the DFG (CRC 183).

-
- [1] R. Sweke, J.-P. Seifert, D. Hangleiter, and J. Eisert, On the quantum versus classical learnability of discrete distributions, *Quantum* **5**, 417 (2021).
 - [2] Y. Liu, S. Arunachalam, and K. Temme, A rigorous and robust quantum speed-up in supervised machine learning, *Nature Phys.* **17**, 1013 (2021).
 - [3] H.-Y. Huang, R. Kueng, and J. Preskill, Information-theoretic bounds on quantum advantage in machine learning, *Phys. Rev. Lett.* **126**, 190505 (2021).
 - [4] N. Pirmay, R. Sweke, J. Eisert, and J.-P. Seifert, Superpolynomial quantum-classical separation for density modeling, *Phys. Rev. A* **107**, 042416 (2023).
 - [5] M. Ragone, B. N. Bakalov, F. Sauvage, A. F. Kemper, C. Ortiz Marrero, M. Larocca, and M. Cerezo, A Lie algebraic theory of barren plateaus for deep parameterized quantum circuits, *Nature Comm.* **15**, 7172 (2024).
 - [6] J. R. McClean, S. Boixo, V. N. Smelyanskiy, R. Babbush, and H. Neven, Barren plateaus in quantum neural network training landscapes, *Nature Comm.* **9**, 4812 (2018).
 - [7] M. Larocca, S. Thanasilp, S. Wang, K. Sharma, J. Biamonte, P. J. Coles, L. Cincio, J. R. McClean, Z. Holmes, and M. Cerezo, A review of barren plateaus in variational quantum computing, *arXiv preprint arXiv:2405.00781* (2024).
 - [8] E. R. Anschuetz and B. T. Kiani, Quantum variational algorithms are swamped with traps, *Nature Comm.* **13**, 7760 (2022).
 - [9] A. A. Mele, A. Angrisani, S. Ghosh, S. Khatri, J. Eisert, D. S. França, and Y. Quek, Noise-induced shallow circuits and absence of barren plateaus, *arXiv preprint arXiv:2403.13927* (2024).
 - [10] N. A. Nemkov, E. O. Kiktenko, and A. K. Fedorov, Barren plateaus are swamped with traps, *arXiv preprint arXiv:2405.05332* (2024).
 - [11] S. Thanasilp, S. Wang, N. A. Nghiem, P. Coles, and M. Cerezo, Subtleties in the trainability of quantum machine learning models, *Quant. Mach. Int.* **5**, 21 (2023).
 - [12] J. Kübler, S. Buchholz, and B. Schölkopf, The inductive bias of quantum kernels, *Advances in Neural Information Processing Systems* **34**, 12661 (2021).
 - [13] M. Cerezo, G. Verdon, H.-Y. Huang, L. Cincio, and P. J. Coles, Challenges and opportunities in quantum machine learning, *Nature Comp. Sc.* **2**, 567 (2022).
 - [14] J. Bowles, V. J. Wright, M. Farkas, N. Killoran, and M. Schuld, Contextuality and inductive bias in quantum machine learning, *arXiv preprint arXiv:2302.01365* (2023).
 - [15] M. Larocca, F. Sauvage, F. M. Sbahi, G. Verdon, P. J. Coles, and M. Cerezo, Group-invariant quantum machine learning, *PRX Quantum* **3**, 030341 (2022).
 - [16] J. J. Meyer, M. Mularski, E. Gil-Fuster, A. A. Mele, F. Arzani, A. Wilms, and J. Eisert, Exploiting symmetry in variational quantum machine learning, *PRX Quantum* **4**, 010328 (2023).
 - [17] J. Bowles, D. Wierichs, and C.-Y. Park, Backpropagation scaling in parameterised quantum circuits, *arXiv preprint arXiv:2306.14962* (2023).
 - [18] C.-Y. Park and N. Killoran, Hamiltonian variational ansatz without barren plateaus, *Quantum* **8**, 1239 (2024).

- [19] S. Jerbi, C. Gyurik, S. C. Marshall, R. Molteni, and V. Dunjko, Shadows of quantum machine learning, *Nature Comm.* **15**, 5676 (2024).
- [20] L. Schatzki, M. Larocca, Q. T. Nguyen, F. Sauvage, and M. Cerezo, Theoretical guarantees for permutation-equivariant quantum neural networks, *npj Quant. Inf.* **10**, 12 (2024).
- [21] P. Rodriguez-Grasa, Y. Ban, and M. Sanz, Training embedding quantum kernels with data re-uploading quantum neural networks, *arXiv preprint arXiv:2401.04642* (2024).
- [22] K. Zhang, L. Liu, M.-H. Hsieh, and D. Tao, Escaping from the barren plateau via Gaussian initializations in deep variational quantum circuits, *Advances in Neural Information Processing Systems* **35**, 18612 (2022).
- [23] H. R. Grimsley, G. S. Barron, E. Barnes, S. E. Economou, and N. J. Mayhall, Adaptive, problem-tailored variational quantum eigensolver mitigates rough parameter landscapes and barren plateaus, *npj Quant. Inf.* **9**, 19 (2023).
- [24] J. Dborin, F. Barratt, V. Wimalaweera, L. Wright, and A. G. Green, Matrix product state pre-training for quantum machine learning, *Quant. Sc. Tech.* **7**, 035014 (2022).
- [25] M. S. Rudolph, J. Miller, D. Motlagh, J. Chen, A. Acharya, and A. Perdomo-Ortiz, Synergistic pretraining of parametrized quantum circuits via tensor networks, *Nature Comm.* **14**, 8367 (2023).
- [26] A. A. Mele, G. B. Mbeng, G. E. Santoro, M. Collura, and P. Torta, Avoiding barren plateaus via transferability of smooth solutions in a Hamiltonian variational ansatz, *Phys. Rev. A* **106**, L060401 (2022).
- [27] R. Puig, M. Drudis, S. Thanasilp, and Z. Holmes, Variational quantum simulation: a case study for understanding warm starts, *arXiv preprint arXiv:2404.10044* (2024).
- [28] Y. Wang, B. Qi, C. Ferrie, and D. Dong, Trainability enhancement of parameterized quantum circuits via reduced-domain parameter initialization, *arXiv preprint arXiv:2302.06858* (2023).
- [29] C.-Y. Park, M. Kang, and J. Huh, Hardware-efficient ansatz without barren plateaus in any depth, *arXiv preprint arXiv:2403.04844* (2024).
- [30] X. Shi and Y. Shang, Avoiding barren plateaus via gaussian mixture model, *arXiv preprint arXiv:2402.13501* (2024).
- [31] Y. Bengio, J. Louradour, R. Collobert, and J. Weston, Curriculum learning, in *Proceedings of the 26th annual international conference on machine learning* (2009) pp. 41–48.
- [32] Q. H. Tran, Y. Endo, and H. Oshima, Quantum curriculum learning, *arXiv preprint arXiv:2407.02419* (2024).
- [33] A. Shrivastava, A. Gupta, and R. Girshick, Training region-based object detectors with online hard example mining, in *Proceedings of the IEEE conference on computer vision and pattern recognition* (2016) pp. 761–769.
- [34] X. Wang, Y. Chen, and W. Zhu, A survey on curriculum learning, *IEEE Trans. Patt. Anal. Mach. Int.* **44**, 4555 (2021).
- [35] P. Soviany, R. T. Ionescu, P. Rota, and N. Sebe, Curriculum learning: A survey, *Int. J. Comp. Vis.* **130**, 1526 (2022).
- [36] R. Tudor Ionescu, B. Alexe, M. Leordeanu, M. Popescu, D. P. Papadopoulos, and V. Ferrari, How hard can it be? Estimating the difficulty of visual search in an image, in *Proceedings of the IEEE Conference on Computer Vision and Pattern Recognition* (2016) pp. 2157–2166.
- [37] S. Guo, W. Huang, H. Zhang, C. Zhuang, D. Dong, M. R. Scott, and D. Huang, Curriculumnet: Weakly supervised learning from large-scale web images, in *Proceedings of the European conference on computer vision (ECCV)* (2018) pp. 135–150.
- [38] L. Jiang, D. Meng, T. Mitamura, and A. G. Hauptmann, Easy samples first: Self-paced reranking for zero-example multimedia search, in *Proceedings of the 22nd ACM international conference on Multimedia* (2014) pp. 547–556.
- [39] E. A. Platanios, O. Stretcu, G. Neubig, B. Póczos, and T. Mitchell, Competence-based curriculum learning for neural machine translation, in *Proceedings of the 2019 Conference of the North American Chapter of the Association for Computational Linguistics: Human Language Technologies* (2019) pp. 1162–1172.
- [40] T. Matiisen, A. Oliver, T. Cohen, and J. Schulman, Teacher–student curriculum learning, *IEEE Trans. Neur. Net. learn. sys.* **31**, 3732 (2019).
- [41] X. Zhang, G. Kumar, H. Khayrallah, K. Murray, J. Gwinnup, M. J. Martindale, P. McNamee, K. Duh, and M. Carpuat, An empirical exploration of curriculum learning for neural machine translation, *arXiv preprint arXiv:1811.00739* (2018).
- [42] A. Pérez-Salinas, A. Cervera-Lierta, E. Gil-Fuster, and J. I. Latorre, Data re-uploading for a universal quantum classifier, *Quantum* **4**, 226 (2020).
- [43] M. Schuld, R. Sweke, and J. J. Meyer, Effect of data encoding on the expressive power of variational quantum-machine-learning models, *Phys. Rev. A* **103**, 032430 (2021).
- [44] G. Penha and C. Hauff, Curriculum learning strategies for IR: An empirical study on conversation response ranking, in *Advances in Information Retrieval* (2020) pp. 699–713.
- [45] M. C. Caro, H.-Y. Huang, M. Cerezo, K. Sharma, A. Sornborger, L. Cincio, and P. J. Coles, Generalization in quantum machine learning from few training data, *Nature Comm.* **13**, 4919 (2022).
- [46] Y. Wu, B. Wu, J. Wang, and X. Yuan, Quantum phase recognition via quantum kernel methods, *Quantum* **7**, 981 (2023).
- [47] Y.-J. Liu, A. Smith, M. Knap, and F. Pollmann, Model-independent learning of quantum phases of matter with quantum convolutional neural networks, *Phys. Rev. Lett.* **130**, 220603 (2023).
- [48] E. Gil-Fuster, J. Eisert, and C. Bravo-Prieto, Understanding quantum machine learning also requires rethinking generalization, *Nature Comm.* **15**, 2277 (2024).
- [49] C. Umeano, A. E. Paine, V. E. Elfving, and O. Kyriienko, What can we learn from quantum convolutional neural networks?, *arXiv preprint arXiv:2308.16664* (2023).
- [50] P. Zapletal, N. A. McMahon, and M. J. Hartmann, Error-tolerant quantum convolutional neural networks for symmetry-protected topological phases, *Phys. Rev. Res.* **6**, 033111 (2024).
- [51] J. Carrasquilla and R. G. Melko, Machine learning phases of matter, *Nature Phys.* **13**, 431–434 (2017).
- [52] S. Sachdev, *Quantum phases of matter* (Cambridge University Press, Massachusetts, 2023).
- [53] R. Verresen, R. Moessner, and F. Pollmann, One-dimensional symmetry protected topological phases and their transitions, *Phys. Rev. B* **96**, 165124 (2017).
- [54] N. Schuch, D. Pérez-García, and I. Cirac, Classifying quantum phases using matrix product states and projected entangled pair states, *Phys. Rev. B* **84**, 165139 (2011).
- [55] A. Elben, J. Yu, G. Zhu, M. Hafezi, F. Pollmann, P. Zoller, and B. Vermersch, Many-body topological invariants from randomized measurements in synthetic quantum matter, *Science advances* **6**, eaaz3666 (2020).
- [56] I. Cong, S. Choi, and M. D. Lukin, Quantum convolutional neural networks, *Nature Phys.* **15**, 1273 (2019).
- [57] E. Recio-Armengol and C. Bravo-Prieto, *Learning complexity gradually in QML models repository*.

- [58] V. Bergholm, J. Izaac, M. Schuld, C. Gogolin, S. Ahmed, V. Ajith, M. S. Alam, G. Alonso-Linaje, B. AkashNarayanan, A. Asadi, *et al.*, PennyLane: Automatic differentiation of hybrid quantum-classical computations, [arXiv preprint arXiv:1811.04968 \(2018\)](#).
- [59] D. P. Kingma, Adam: A method for stochastic optimization, [arXiv preprint arXiv:1412.6980 \(2014\)](#).
- [60] G. Aguilar, S. Cichy, J. Eisert, and L. Bittel, Full classification of Pauli Lie algebras, [arXiv preprint arXiv:2408.00081 \(2024\)](#).
- [61] D. Gross, K. M. R. Audenaert, and J. Eisert, Evenly distributed unitaries: on the structure of unitary designs, *J. Math. Phys.* **48**, 052104 (2007).
- [62] M. L. Goh, M. Larocca, L. Cincio, M. Cerezo, and F. Sauvage, Lie-algebraic classical simulations for variational quantum computing, [arXiv preprint arXiv:2308.01432 \(2023\)](#).
- [63] M. Larocca, P. Czarnik, K. Sharma, G. Muralidharan, P. J. Coles, and M. Cerezo, Diagnosing barren plateaus with tools from quantum optimal control, *Quantum* **6**, 824 (2022).
- [64] L. Cincio, Y. Subaşı, A. T. Sornborger, and P. J. Coles, Learning the quantum algorithm for state overlap, *New Journal of Physics* **20**, 113022 (2018).
- [65] K. Beer, D. Bondarenko, T. Farrelly, T. J. Osborne, R. Salzmann, D. Scheiermann, and R. Wolf, Training deep quantum neural networks, *Nature Comm.* **11**, 808 (2020).
- [66] L. Cincio, K. Rudinger, M. Sarovar, and P. J. Coles, Machine learning of noise-resilient quantum circuits, *PRX Quantum* **2**, 010324 (2021).
- [67] Z. Yu, X. Zhao, B. Zhao, and X. Wang, Optimal quantum dataset for learning a unitary transformation, *Phys. Rev. Applied* **19**, 034017 (2023).
- [68] D. F. Locher, L. Cardarelli, and M. Müller, Quantum error correction with quantum autoencoders, *Quantum* **7**, 942 (2023).
- [69] S. Shalev-Shwartz and S. Ben-David, *Understanding machine learning: From theory to algorithms* (Cambridge university press, 2014).

Appendix A: Proof of Proposition 1

In this section, we re-state and prove Proposition 1.

Proposition 1 (Mitigation of barren plateaus). *Let $\{|\psi_i\rangle \in \mathcal{H}\}$ be a collection of quantum state vectors. Let $f_{\vartheta} : \mathcal{H} \rightarrow \mathcal{Y}$ be a parameterized quantum model with parameters $\vartheta \in \Theta$ and $\mathcal{Y} \subseteq \mathbb{R}$ the label space. Consider a loss function $\ell(\vartheta; (|\psi\rangle, y))$ associated with data points $\{(|\psi_i\rangle, y_i) \in \mathcal{H} \times \mathcal{Y}\}$. Suppose there exists a scoring function $s : \mathcal{H} \rightarrow [0, 1]$ such that the expected squared norm of the gradient*

$$G(z) = \mathbb{E} \left[\|\nabla_{\vartheta} \ell(\vartheta; (|\psi\rangle, y))\|^2 \mid s(\psi) = z \right] \quad (\text{A1})$$

is a non-increasing function of s . Then, this learning setup defined by s increases the expected squared gradient magnitude during early training epochs compared to standard training (random data order).

Proof. Let F be the cumulative distribution function of the scores over the data set given by

$$F(z) = \mathbb{P} [s(\psi_i) \leq z]. \quad (\text{A2})$$

The learner has access to the subset $\mathcal{D}_t = \{(|\psi_i\rangle, y_i) \mid s(\psi_i) \leq z_t\}$. The expected gradient magnitude at epoch t is defined as

$$\mathbb{E}_{\mathcal{D}_t} [\|g\|^2] = \frac{1}{F(z_t)} \int_0^{z_t} G(z) dF(z), \quad (\text{A3})$$

where g is the gradient of the loss function with respect to the parameters ϑ . For random data presentation, all data points are equally likely to be sampled, regardless of their scores. Therefore,

$$\mathbb{E}_{\text{rand}} [\|g\|^2] = \int_0^1 G(z) dF(z). \quad (\text{A4})$$

Since G is non-increasing, for $z \leq z_t$, $G(z) \geq G(z_t)$, and similarly, for $z \geq z_t$, $G(z) \leq G(z_t)$. Therefore, we can lower bound

$$\mathbb{E}_{\mathcal{D}_t} [\|g\|^2] \geq \frac{1}{F(z_t)} G(z_t) \int_0^{z_t} dF(z) = G(z_t), \quad (\text{A5})$$

and upper bound

$$\mathbb{E}_{\text{rand}} [\|g\|^2] \leq G(z_t) F(z_t) + G(z_t) (1 - F(z_t)) = G(z_t), \quad (\text{A6})$$

which leads to

$$\mathbb{E}_{\mathcal{D}_t} [\|g\|^2] \geq \mathbb{E}_{\text{rand}} [\|g\|^2], \quad (\text{A7})$$

which proves the statement to be shown. \square

Appendix B: Proof of Proposition 2

In this section, we re-state and prove Proposition 2.

Proposition 2 (Faster convergence). *Let $\{|\psi_i\rangle\} \in \mathcal{H}$ be a collection of quantum state vectors. Let $f_{\vartheta} : \mathcal{H} \rightarrow \mathcal{Y}$ be a parameterized quantum model with parameters $\vartheta \in \Theta$ and $\mathcal{Y} \subseteq \mathbb{R}$ the label space. Consider a convex loss function with Lipschitz continuous gradients $\ell(\vartheta; (|\psi\rangle, y))$ associated with data points $\{(|\psi_i\rangle, y_i) \in \mathcal{H} \times \mathcal{Y}\}$. Suppose there exists a scoring function $s : \mathcal{H} \rightarrow [0, 1]$ such that the scoring function $s(|\psi\rangle)$ prioritizes data points with lower gradient variance at each epoch, and the pacing function p increases monotonically over epochs $t = 1$ to T . Then, this learning setup defined by s and p results in a lower expected empirical risk after T epochs compared to standard training (random data order), i.e.,*

$$\mathbb{E}[R(\vartheta_T^{s,p})] \leq \mathbb{E}[R(\vartheta_T^{\text{rand}})] \quad (\text{B1})$$

where $R(\vartheta) := \frac{1}{N} \sum_{i=1}^N \ell(f_{\vartheta}; (|\psi_i\rangle, y_i))$ is the empirical risk, and N the batch size.

Proof. In standard training, data points are selected uniformly at random. The variance of the stochastic gradient is

$$\sigma_{\text{rand}}^2 = \mathbb{E}_{(|\psi\rangle, y) \sim D} [\|\nabla \ell(f_{\vartheta}; (|\psi\rangle, y)) - \nabla R(\vartheta)\|^2] \quad (\text{B2})$$

where D is the uniform distribution over the entire dataset. In contrast, for the learning setup defined by s and p , the variance of the stochastic gradient is

$$\sigma_{s,p}^2 = \mathbb{E}_{(\psi,y) \sim D_t} [\|\nabla \ell(f_{\boldsymbol{\vartheta}_t}; (\psi), y) - \nabla R(\boldsymbol{\vartheta}_t)\|^2] \quad (\text{B3})$$

where

$$\mathcal{D}_t = \{(\psi_i), y_i \mid s(\psi_i) \leq z_t\}. \quad (\text{B4})$$

For convex functions with Lipschitz continuous gradients, the expected suboptimality after T epochs is bounded by [69]

$$\mathbb{E}[R(\boldsymbol{\vartheta}_T) - R(\boldsymbol{\vartheta}^*)] \leq \frac{\|\boldsymbol{\vartheta}_0 - \boldsymbol{\vartheta}^*\|^2}{2\eta T} + \frac{\eta}{2T} \sum_{t=1}^T \sigma^2(t), \quad (\text{B5})$$

where $\boldsymbol{\vartheta}_0$ are the initial parameters, $\boldsymbol{\vartheta}^*$ are the optimal parameters minimizing $R(\boldsymbol{\vartheta})$, and η is the learning rate (which we assume to be constant for simplicity). Then, for the standard

training we have

$$\mathbb{E}[R(\boldsymbol{\vartheta}_T^{\text{rand}}) - R(\boldsymbol{\vartheta}^*)] \leq \frac{\|\boldsymbol{\vartheta}_0 - \boldsymbol{\vartheta}^*\|^2}{2\eta T} + \frac{\eta}{2T} \sum_{t=1}^T \sigma_{\text{rand}}^2(t), \quad (\text{B6})$$

and for the setup defined by s and t

$$\mathbb{E}[R(\boldsymbol{\vartheta}_T^{s,p}) - R(\boldsymbol{\vartheta}^*)] \leq \frac{\|\boldsymbol{\vartheta}_0 - \boldsymbol{\vartheta}^*\|^2}{2\eta T} + \frac{\eta}{2T} \sum_{t=1}^T \sigma_{s,p}^2(t). \quad (\text{B7})$$

Given that for all t , $\sigma_{s,p}^2(t) \leq \sigma_{\text{rand}}^2(t)$, it follows that

$$\sum_{t=1}^T \sigma_{s,p}^2(t) \leq \sum_{t=1}^T \sigma_{\text{rand}}^2(t). \quad (\text{B8})$$

Combining these inequalities, we obtain

$$\mathbb{E}[R(\boldsymbol{\vartheta}_T^{s,p}) - R(\boldsymbol{\vartheta}^*)] \leq \mathbb{E}[R(\boldsymbol{\vartheta}_T^{\text{rand}}) - R(\boldsymbol{\vartheta}^*)], \quad (\text{B9})$$

which results in

$$\mathbb{E}[R(\boldsymbol{\vartheta}_T^{s,p})] \leq \mathbb{E}[R(\boldsymbol{\vartheta}_T^{\text{rand}})]. \quad (\text{B10})$$

□